

Enhanced coherence in superconducting circuits via band engineering

Luca Chiroli^{1,2} and Joel E. Moore^{1,3}

¹*Department of Physics, University of California, Berkeley, CA 94720*

²*Istituto Nanoscienze - CNR, I-56127 Pisa*

³*Materials Sciences Division, Lawrence Berkeley National Laboratory, Berkeley, CA 94720*

In superconducting circuits interrupted by Josephson junctions, the dependence of the energy spectrum on offset charges on different islands is $2e$ periodic through the Aharonov-Casher effect and resembles a crystal band structure that reflects the symmetries of the Josephson potential. We show that higher-harmonic Josephson elements described by a $\cos(2\varphi)$ energy-phase relation provide an increased freedom to tailor the shape of the Josephson potential and design spectra featuring multiplets of flat bands and Dirac points in the charge Brillouin zone. Flat bands provide noise-insensitive quantum states, and band engineering can help improve the coherence of the system. We discuss a modified version of a flux qubit that achieves in principle no decoherence from charge noise and introduce a flux qutrit that shows a spin-one Dirac spectrum and is simultaneously quite robust to both charge and flux noise.

Introduction.— Superconducting circuits are among the best candidates for quantum computation applications [1–3] and represent an ideal platform for the study and the implementation of artificial quantum matter [4, 5]. Among the several varieties, the superconducting flux qubit (FQ) [6] represents one of the early prototypes [7–9], and has recently received renewed interest [10–12]. Its two fundamental current-carrying states correspond to the minima of the circuit Josephson potential, and quantum tunneling (phase slip) generates coherent superpositions. Due to the Aharonov-Casher effect [13, 14], the spectrum of the qubit acquires a dependence on gate-controlled offset charges localized on the islands between the junctions. The charge degeneracy of the condensate confers a $2e$ periodicity to the spectrum, which resembles a crystal band structure [6, 15–17]. In a small loop hosting n independent superconducting islands, the spectrum in the n dimensional charge Brillouin zone (BZ) can potentially host Dirac and Weyl points [17] or flat bands, thus simulating quantum materials. An analogous and dual approach has been recently put forward, where the Andreev spectrum of a multi-terminal Josephson junction can host Weyl points and can be seen as a kind of topological matter [18, 19].

Typically the dependence on the offset charges is minimized as one of the main source of decoherence in superconducting qubits is represented by charge noise [6, 20–22]. This is the case of the transmon qubit design [23–25] where a large capacitance shunts a small superconducting island, resulting in band flattening as a function of the offset charges, at the price of weakly anharmonic spectra. The same idea has been employed in the later versions of the flux qubit, where a shunt capacitance reduces charge sensitivity [10–12]. On the other hand, drawing from the analogy with crystal band structures, flattening of the bands can result from destructive interference. This is the case in the flat bands of twisted bilayer graphene [26–28], which have recently attracted enormous interest, or the quantum Hall effect, where long-wavelength destruc-

tive interference quenches the kinetic energy. A short wavelength counterpart is represented by lattice models such as the Lieb or the Kagome lattice, where an atomic redundancy at the unit cell level typically produces flat bands. Spectra featuring multiplets of flat bands provide noise-insensitive quantum states, without paying the price of weak anharmonicity.

The compactness of the superconducting phase rules out long wavelength perturbations but does not forbid short wavelength modulations. To achieve multiplets of flat bands, an ordinary Josephson junction described by a $\cos(\varphi)$ energy-phase relation alone is not sufficient to tailor at will the details of a structured unit cell. We can, however, employ higher-harmonic effective Josephson junctions, such as a $-E_{4e} \cos(2\varphi)$ energy-phase relation, which effectively describes tunneling of pairs of Cooper pairs. A variety of π -periodic energy-phase relations have been recently proposed [29, 30]. An effective $\cos(2\varphi)$ is realized through gatemons [31, 32] based on semiconducting wires [33, 34], or can be obtained by using four nominally equal JJs in a rhombus configuration [35–39]. In turn, the recently introduced bifluxon qubit [40], defined by the parity of the flux quanta, is based on an effective $\cos(\varphi/2)$ energy-phase relation. These elements provide us with augmented freedom to engineer the Josephson potential and increase the coherence of the system.

We discuss a modified flux qubit that displays multiplets of levels that hardly depend on the offset charges, thus rendering the device basically insensitive to charge noise. In turn, by increasing the sensitivity to the offset charges, we discuss an implementation of a three-band model mimicking a Lieb lattice and define a flux qutrit featuring a single Dirac cone and an almost flat band in the charge BZ. Despite the increased sensitivity to offset charges, this device shows a good degree of robustness to charge noise and, perhaps more interestingly, an increased insensitivity to flux noise compared to conventional flux qubits.

Charge Noise Insensitive FQ.— The low energy Hamiltonian of a flux qubit is written in terms of opposite current carrying states, $|L\rangle$ and $|R\rangle$, that corresponds to the two minima of the Josephson potential, that is depicted in Fig. 1b). Quantum mechanical tunneling between the minima generates a coherent off-diagonal finite matrix element $\Delta = \langle L|H|R\rangle$. A quantum tunneling accompanied by a 2π quantum phase slip acquires a dependence on the offset charges via the Aharonov-Casher effect. In an extended picture of the Josephson potential, the low energy Hamiltonian can be constructed via a tight binding model, where the role of the momentum is played by the offset charges $q_1 = Q_1/2e$ and $q_2 = Q_2/2e$. This way, after recognizing a deformed honeycomb lattice structure, the off-diagonal matrix element is written as $\Delta_{\mathbf{q}} = -\Delta_0 - t_1(e^{2\pi i Q_1/2e} + e^{2\pi i Q_2/2e})$, in terms of hoppings Δ_0 and t_1 . The FQ Hamiltonian then reads

$$H = \epsilon(\varphi_x)\sigma_z - \Delta_{\mathbf{q}}\sigma^+ - \Delta_{\mathbf{q}}^*\sigma^-, \quad (1)$$

with $\epsilon(\varphi_x)$ an energy imbalance between the two current carrying states, and $\varphi_x = \Phi_x/2\pi$ the flux threading the loop set at $\Phi_x = \Phi_0/2$. A two-dimensional Dirac spectrum gapped by $\epsilon(\varphi_x)$ emerges for $t_1 > t_0$ [6, 15–17].

Typically, in order to increase robustness to charge noise the potential barrier between different cells is increased by reducing the area of one Josephson junction. We now show that we can suppress the tunneling in another way. Suppose we only have $\cos(2\varphi)$ JJs. The FQ Josephson potential will simply acquire a π periodicity and two branches of $4e$ periodic spectra will appear, one for even and one for odd number of Cooper pairs, shifted by $2e$. If we now shunt the two nominally equal π -periodic JJs with ordinary 2π -periodic JJs with smaller energy we create a modulation of the Josephson potential on the scale of the 2π periodicity.

The full circuit is schematically depicted in Fig. 1a). A shunt capacitance on the third, nominally different, JJ helps reducing sensitivity on the sum (difference) of the offset charges [10]. Denoting with $\gamma = (C'_J + C_s)/C$ the capacitances ratio, the full Hamiltonian reads

$$H = 4E_C(-i\nabla_{\varphi} + \mathbf{q})^T C^{-1}(-i\nabla_{\varphi} + \mathbf{q}) + V(\varphi), \quad (2)$$

with $q_i = C_g V_i/2e$, $E_C = e^2/2C$, $C = C_J + C_g$, and the symmetric capacitance matrix specified by $C_{ii} = 1 + \gamma$ and $C_{12} = \gamma$. The Josephson potential is

$$V(\varphi) = - \sum_{i=1,2} (E_{2e} \cos(\varphi_i) + E_{4e} \cos(2\varphi_i)) - E'_{4e} \cos(2(\varphi_x - \varphi_1 - \varphi_2)), \quad (3)$$

where E_{2e} stands for the ordinary Josephson energy. The potential for the choice $\phi_x = \pi/2$ is shown in Fig. 1d): two absolute minima are at the center of the unit cell and the adjacent minima, corresponding to π shifted replica, are higher in energy as an effect of the 2π modulation.

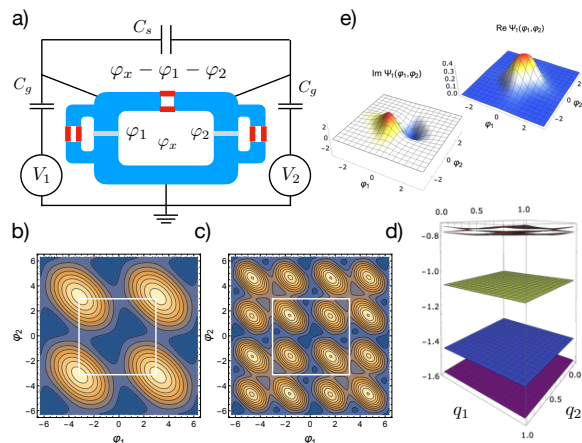


FIG. 1. a) Schematics of a variation of flux qubit employing $\cos(2\varphi)$ JJs. b,c) Josephson potential of b) an ordinary Flux Qubit and c) Eq. (3) for the choice $\alpha = 0.8$ and $\beta = 0.2$. The unit cell containing three minima is highlighted in white. d) Exact spectrum showing the six lowest energy level as a function of the two offset charges q_1 and q_2 . e) Unnormalized wavefunction of the first two levels at $q_1 = q_2 = 0$.

Tunneling to the next unit cell necessarily has to take place via virtual processes through secondary minima. Denoting by Δ_0 and δ_1 the intracell tunneling matrix element between absolute and relative minima, respectively, and t_1 the intercell tunneling matrix elements, with $t_1 < \delta_1 < \Delta_0$, at second order perturbation theory we have

$$\Delta_{\mathbf{q}} = \Delta_0 + \frac{\delta_1 t_1^2}{\delta E^2 - \delta_1^2} (e^{2\pi i q_1} + e^{2\pi i q_2}), \quad (4)$$

with δE the energy difference between the central absolute minima and the relative minima. Clearly, δE dominates over Δ_0 , as the former is on order of E_{2e} whereas the latter is due to a tunneling process. In the limit $\delta_1, t_1 \ll \Delta_0 \ll \delta E$ the dependence on the offset charges becomes highly suppressed.

The predictions of the low energy tight-binding model are checked by diagonalization of the full Hamiltonian in the charge basis and the six lowest energy bands are shown in Fig. 1d). The spectrum has been calculated assuming $\gamma = 1.9$, $\alpha = E'_{4e}/E_{4e} = 0.8$, $\beta = E_{2e}/E_{4e} = 0.5$, and $E_C/E_{4e} = 0.055$. We see that on the scale of the full $2e$ charge BZ the lowest three bands are basically flat. The wavefunctions of the lowest two energy levels are shown in Fig. 1e) confirm symmetric and antisymmetric superposition of current carrying states.

We now fully address the coherence of the device to charge and flux fluctuations. The general coupling of a fluctuating classical variable $\delta\lambda_i(t)$ to the circuits reads [20–22]

$$H_{\text{int}} = \sum_i \delta\lambda_i(t) \mathcal{O}_i. \quad (5)$$

with $\mathcal{O}_i = \partial H / \partial \lambda_i$ the operator that couples to the variable λ_i in the Hamiltonian H in Eq. (2). Charge fluctuations couple to the dimensionless charge operator $\hat{Q}_i = 8E_C \mathcal{C}_{ij}^{-1} (-i\partial_j + q_j)$ and flux fluctuations couple to the current operator $I = \frac{2\pi}{\Phi_0} \partial V / \partial \varphi_x$. Singling out the two lowest energy states, we define the qubit energy basis $|0\rangle$ and $|1\rangle$, and a set of Pauli matrices such that $\sigma_z|0\rangle = -|0\rangle$. The relaxation time is typically estimated by treating the environment as a perturbation and takes the Fermi golden rule expression

$$\frac{1}{T_1} = \frac{1}{\hbar^2} \sum_i |\langle 0 | \mathcal{O}_i | 1 \rangle|^2 S_i(\omega_{01}), \quad (6)$$

where $S_i(\omega)$ is the environment power spectrum defined as $S_i(\omega) = \int d\tau e^{-i\omega\tau} \langle \delta\lambda_i(t+\tau) \delta\lambda_i(t) \rangle$ and $\omega_{01} = (E_1 - E_0)/\hbar$. The pure dephasing time appears in the time evolution of the coherent superposition $|0\rangle + \langle e^{i\delta\phi_{01}(t)} | 1 \rangle$, with $\delta\phi_{01}(t) = \int_0^t dt' \omega_{01}(t')$. After statistical average over the fluctuating field and assuming Gaussian noise we have $e^{-\Gamma_\phi(t)} \equiv \langle e^{i\delta\phi_{01}(t)} \rangle = \exp[-\frac{1}{2} \langle \delta\phi_{01}^2(t) \rangle]$, so that [22, 41, 42]

$$\Gamma_\phi(t) = \sum_i |\langle 1 | \mathcal{O}_i | 1 \rangle - \langle 0 | \mathcal{O}_i | 0 \rangle|^2 F_i(t), \quad (7)$$

where $F_i(t) = \frac{1}{\hbar^2} \int_{\omega_c}^{\infty} \frac{d\omega}{2\pi} S_i(\omega) \frac{\sin^2(\omega t/2)}{(\omega/2)^2}$ and ω_c is a low-frequency cutoff. The decay for short time is Gaussian, the pure dephasing time T_ϕ is defined as $\Gamma_\phi(T_\phi) = 1$ and strongly depends on the functions $F_i(t)$. In what follows, we approximate $F_i(t)$ to one, which is the worst case scenario [42]. Given the form of the relaxation and dephasing rate, two strategies are typically employed to reduce them: either reduce the coupling to the environment, or reduce the fluctuations in the environment. Here we follow the first route and assess the matrix elements of the charge and current operators in the qubit basis.

Pure dephasing can be assessed by directly looking at the dependence of the qubit frequency ω_{01} on charge and flux. In Fig. 3 we plot the energy difference as a function of the normalized charges on the entire charge BZ. At the sweet spot $q_i = 0, 1/2$ the derivative is exactly zero. More interesting is the bandwidth of energy variation in Fig. 2a), from which it follows that $4\delta_1 t_1^2 / (\Delta_0 (\delta E^2 - \delta_1^2)) \simeq 10^{-5}$. This way, $T_1^{-1} \propto 10^{-10} \Delta_0^2 S_q(\Delta_0)$ and $T_\phi^{-1} < 10^{-5} \Delta_0$. We can then conclude that the dephasing time due to charge fluctuations is on order of hundreds of microseconds in the worst cases. Flux qubits are clearly very susceptible to flux noise due to the intrinsic dependence of the Josephson potential on the external flux. The latter controls the value of the circulating current and couples directly to one qubit axis in Eq. (1). It immediately follows that the relaxation rate T_1^{-1} has a maximum at $\varphi_x = \pi/2$, for which $\epsilon(\varphi_x) = 0$ and the perturbation is purely off diagonal. At the same time, the point $\varphi_x = \pi/2$ represents a sweet spot of formally

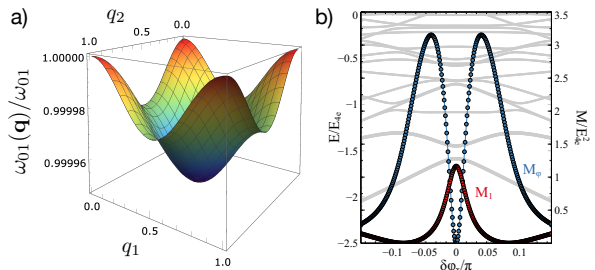


FIG. 2. a) Energy difference between the two qubit states as a function of the normalized gate charges. b) Full spectrum highlighting the two lowest energy levels as a function of the applied flux $\delta\varphi_x = \varphi_x - \pi/2$ and matrix elements M_ϕ and M_1 determining the relaxation and pure decoherence rates.

infinite pure dephasing time T_ϕ and qubit operations can be performed at twice the qubit frequency [43, 44]. To estimate the relaxation rate we note that the circulating current in the setup is twice the one typically circulating in a flux qubit, due to the doubled periodicity of the Josephson potential. This way, the relaxation rate is nominally four times larger than the typical FQ case. The exact matrix elements $M_\phi = (\Phi_0/2\pi)^2 |I_{00} - I_{11}|^2$ and $M_1 = (\Phi_0/2\pi)^2 |I_{01}|^2$ determining the dephasing and relaxation rates are shown in Fig. 2b), together with the circuit spectrum, versus the applied flux. It follows that away from the sweet spot dephasing due to flux noise can severely affect the device performances.

Flux qutrit. — We now explain how a qutrit design can retain a high degree of robustness to charge noise, as in the above circuit, while having a reduced sensitivity to flux noise. We consider the system shown in Fig. 3a). It is composed by a flux qubit where two junctions are shunted each by a π -periodic JJ. The two new effective junctions are described by the effective potential

$$V_{\text{eff}}(\varphi) = -E_{2e} \cos(\varphi_0 - \varphi) - E_{4e} \cos(2\varphi), \quad (8)$$

where φ_0 is the flux threading the loop between the two elements. The Hamiltonian has the form of Eq. (2), with the Josephson potential given by

$$V(\varphi) = - \sum_{i=1,2} (E_{2e} \cos(\varphi_i) + E_{4e} \cos(2\varphi_i)) - E'_{2e} \cos(\varphi_x - \varphi_1 - \varphi_2), \quad (9)$$

where we assumed the two effective junctions to be equal, the third to have Josephson energy E'_{2e} , and we set $\varphi_0 = 0$. For the choice $\varphi_x = \pi$ the Josephson potential has three minima in the unit cell, two degenerate and one relative, as shown in Fig. 3b). Their relative energy can be tuned by varying $\alpha = E_{2e}/E_{4e}$ and $\beta = E'_{2e}/E_{4e}$ and for $\alpha = \beta$ the three minima are degenerate. In order to be good fundamental states their energy difference must be smaller than the plasma frequency $\omega_P = \sqrt{4E_C E_{4e}}$.

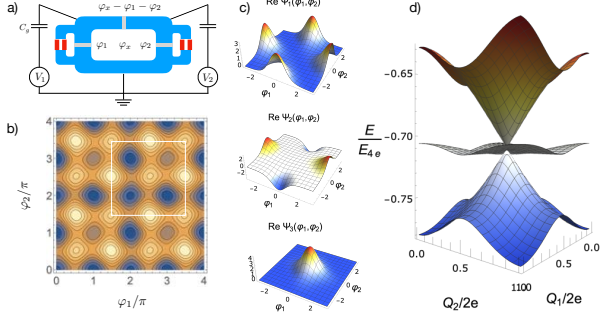


FIG. 3. a) Schematics of a variation of flux qubit whose spectrum realizes a flux qutrit. b) Josephson potential of Eq. (9) for the choice $\alpha = 0.3$ and $\beta = 0.4$. The unit cell containing three minima is highlighted in white. c) Unnormalized wavefunction of the first three levels at $q_1 = q_2 = 1/2$. d) Exact spectrum showing the three lowest energy level as a function of the two offset charges Q_1 and Q_2 .

This requires that the $4e$ Josephson element dominate, with $\alpha, \beta < 1$. On the other hand, too small a value of α calls into play a fourth minimum that would trivialize the analysis. Small values of β ensure that only three fundamental minima determine the low energy physics.

The three minima define a flux qutrit and form a Lieb lattice in an extended picture of the potential. It is instructive to construct a minimal tight-binding model to describe the low energy bands. The potential Eq. (9) breaks "mirror" symmetry, $V(-\varphi_1, \varphi_2) \neq V(\varphi_1, \varphi_2)$ and $V(\varphi_1, -\varphi_2) \neq V(\varphi_1, \varphi_2)$, so that two fundamental hoppings t_0 and t_1 can be introduced. A third hopping t_2 has to be introduced in order to account for tunneling through the barrier between two degenerate minima. The effective Hamiltonian reads

$$H_{\mathbf{q}} = \begin{pmatrix} 0 & T(q_1) & \tilde{T}_{\mathbf{q}} \\ T^*(q_1) & -\epsilon(\varphi_x) & T^*(q_2) \\ \tilde{T}_{\mathbf{q}}^* & T(q_2) & 0 \end{pmatrix}, \quad (10)$$

with $T(q) = -t_0 - t_1 e^{-2\pi i q}$ and $\tilde{T}_{\mathbf{q}} = -t_2(1 + e^{2\pi i(q_1 - q_2)})$. For $t_0 = t_1$ and $\epsilon = t_2 = 0$, the spectrum realizes a well known spin 1 Dirac Hamiltonian, with three degenerate states at $q_1 = q_2 = 1/2$, a flat band and a Dirac cone at the center of the charge BZ. Both $\epsilon \neq 0$ and $t_0 \neq t_1$ open a finite gap in the spectrum. For $t_2 = 0$ the model always contains a flat band given by the state

$$u_{\mathbf{q}}^0 = \begin{pmatrix} t_0 + t_1 e^{2\pi i q_2} \\ 0 \\ -t_0 - t_1 e^{2\pi i q_1} \end{pmatrix}. \quad (11)$$

For $t_2 \neq 0$ the flat band acquires a weak dispersion and two symmetry protected Dirac points develops at its crossing with one of the other two bands. The parameters t_0 , t_1 and t_2 depend on the potential barriers and the effective capacitances of the circuit. Fine tuning is possible through flux-dependent Josephson junctions. We

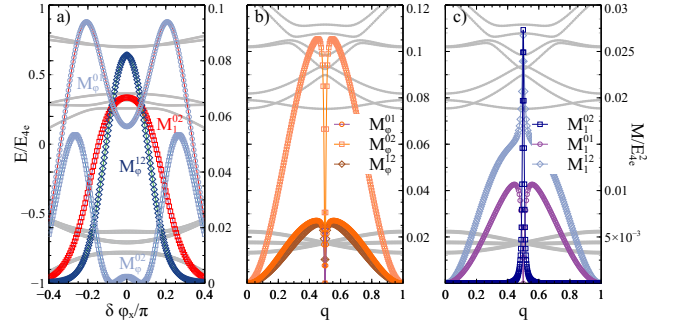


FIG. 4. Back panels: lowest energy spectrum of a flux qutrit as a function of: a) the flux bias $\delta\varphi_x = \varphi_x - \pi/2$, and b,c) the normalized offset charges $q_1 = -q_2 = q$. Front panels: associated matrix elements determining the relaxation and pure decoherence rates: a) M_ϕ and M_1 versus $\delta\varphi_x$, b) M_ϕ and c) M_1 versus q .

numerically diagonalize the Hamiltonian in the charge basis and the low energy spectrum is shown in Fig. 3d) for $\alpha = 0.3$, $\beta = 0.352$, and $E_C/E_{2e} = 0.1$. An approximate spin 1 Dirac spectrum is obtained, with dispersive conduction and valence bands and an approximately flat band, with deviations due to finite hopping t_2 between degenerate minima. The wave functions at $q_1 = q_2 = 1/2$ is shown in Fig. 1d) and symmetric and anti-symmetric combinations of the two degenerate minima appear.

The flux qutrit so far defined shows interesting coherence properties. Analogously to the case of a qubit we can define qutrit dephasing and relaxation rates between different levels, $\Gamma_\phi^{nm}(t) = \sum_i |\langle n|\mathcal{O}_i|n\rangle - \langle m|\mathcal{O}_i|m\rangle|^2 F_i(t)$ and $\Gamma_1^{nm} = \frac{1}{\hbar^2} \sum_i |\langle n|\mathcal{O}_i|m\rangle|^2 S_i(\omega_{nm})$, and associated matrix elements $M_{1,\phi}^{nm}$, that generically describe the influence of the environment. Clearly the sensitivity to charge noise is enhanced, as shown in Fig. 4b,c). The point $q_1 = q_2 = 0$ represents a sweet spot. Dephasing and relaxation rates all increase towards the center of the charge BZ. M_ϕ^{nm} all show a dip at the Dirac point, due to level coalescence and only one M_1^{01} shows a dip, signaling a transition decoupling.

More interesting is the sensitivity to flux noise. In Fig. 4a) we plot the dependence of the relevant matrix elements, together with the lowest energy level of the device, as a function of the applied flux φ_x at $\mathbf{q} = 0$. We notice that only the energy of the flatband is sensitive to the applied flux in a good flux window. We then notice that $\Gamma_1^{01} = \Gamma_1^{12} = 0$ within numerical precision. This is due to the fact that the flux in Eq. (10) couples only states $|0\rangle$ and $|2\rangle$. It also follows that, as for the case of the FQ previously described, the associated dephasing rate Γ_ϕ^{02} reaches minimum when Γ_1^{02} is a maximum. In turn, Γ_ϕ^{01} and Γ_ϕ^{12} are nonzero in the energy window in which only the flatband energy varies with the flux and Γ_1^{02} is activated only at the Dirac point. Importantly, we notice that the scale of the squared matrix element is

nominally two orders of magnitude smaller than in the case of the flux qubit in Fig. 2.

The matrix elements $M_{1,\phi}^{nm}$ also give information on the accessibility of the quantum states by external means for quantum computing manipulations. We notice a complementarity between charge and flux dependence and complete access to the low energy subspace is provided by $M_1^{02}(\varphi_x)$, $M_1^{01}(\mathbf{q})$, $M_1^{12}(\mathbf{q})$. Our results show that the modification of conventional superconducting circuits to include two types of Josephson junction current-phase relations, both of current interest, can allow significant gains in robustness to both charge and flux noise, providing a path beyond current limitations of flux qubits.

Acknowledgments.— The authors are grateful to N. Yao for very useful discussions. L.C. acknowledges the European Commission for funding through the MCSA Global Fellowship grant TOPOCIRCUS-841894. J.E.M. was supported by the U.S. Department of Energy, Office of Science through the Quantum Science Center (QSC), a National Quantum Information Science Research Center.

-
- [1] M. H. Devoret and R. J. Schoelkopf, *Science* **339**, 1169 (2013).
- [2] J. Preskill, *Quantum* **2**, 79 (2018).
- [3] M. Kjaergaard, M. E. Schwartz, J. Braumüller, P. Krantz, J. I.-J. Wang, S. Gustavsson, and W. D. Oliver, *Annual Review of Condensed Matter Physics* **11**, 369 (2020).
- [4] A. Kandala, A. Mezzacapo, K. Temme, M. Takita, M. Brink, J. M. Chow, and J. M. Gambetta, *Nature* **549**, 242 (2017).
- [5] F. Arute, K. Arya, R. Babbush, D. Bacon, J. C. Bardin, R. Barends, S. Boixo, M. Broughton, B. B. Buckley, D. A. Buell, B. Burkett, N. Bushnell, Y. Chen, Z. Chen, B. Chiaro, R. Collins, W. Courtney, S. Demura, A. Dunsworth, E. Farhi, A. Fowler, B. Foxen, C. Gidney, M. Giustina, R. Graff, S. Habegger, M. P. Harrigan, A. Ho, S. Hong, T. Huang, W. J. Huggins, L. Ioffe, S. V. Isakov, E. Jeffrey, Z. Jiang, C. Jones, D. Kafri, K. Kechedzhi, J. Kelly, S. Kim, P. V. Klimov, A. Korotkov, F. Kostritsa, D. Landhuis, P. Laptev, M. Lindmark, E. Lucero, O. Martin, J. M. Martinis, J. R. McClean, M. McEwen, A. Megrant, X. Mi, M. Mohseni, W. Mruczkiewicz, J. Mutus, O. Naaman, M. Neeley, C. Neill, H. Neven, M. Y. Niu, T. E. O’Brien, E. Ostby, A. Petukhov, H. Putterman, C. Quintana, P. Roushan, N. C. Rubin, D. Sank, K. J. Satzinger, V. Smelyanskiy, D. Strain, K. J. Sung, M. Szalay, T. Y. Takeshita, A. Vainsencher, T. White, N. Wiebe, Z. J. Yao, P. Yeh, and A. Zalcman, *Science* **369**, 1084 (2020).
- [6] T. P. Orlando, J. E. Mooij, L. Tian, C. H. van der Wal, L. S. Levitov, S. Lloyd, and J. J. Mazo, *Phys. Rev. B* **60**, 15398 (1999).
- [7] J. E. Mooij, T. P. Orlando, L. Levitov, L. Tian, C. H. van der Wal, and S. Lloyd, *Science* **285**, 1036 (1999).
- [8] C. H. van der Wal, A. C. J. ter Haar, F. K. Wilhelm, R. N. Schouten, C. J. P. M. Harmans, T. P. Orlando, S. Lloyd, and J. E. Mooij, *Science* **290**, 773 (2000).
- [9] I. Chiorescu, Y. Nakamura, C. J. P. M. Harmans, and J. E. Mooij, *Science* **299**, 1869 (2003).
- [10] J. Q. You, X. Hu, S. Ashhab, and F. Nori, *Phys. Rev. B* **75**, 140515 (2007).
- [11] F. Yan, S. Gustavsson, A. Kamal, J. Birenbaum, A. P. Sears, D. Hover, T. J. Gudmundsen, D. Rosenberg, G. Samach, S. Weber, J. L. Yoder, T. P. Orlando, J. Clarke, A. J. Kerman, and W. D. Oliver, *Nature Communications* **7**, 12964 (2016).
- [12] L. V. Abdurakhimov, I. Mahboob, H. Toida, K. Kakuyanagi, and S. Saito, *Applied Physics Letters* **115**, 262601 (2019), <https://doi.org/10.1063/1.5136262>.
- [13] Y. Aharonov and A. Casher, *Phys. Rev. Lett.* **53**, 319 (1984).
- [14] W. J. Elion, J. J. Wachtters, L. L. Sohn, and J. E. Mooij, *Phys. Rev. Lett.* **71**, 2311 (1993).
- [15] L. Chiroli and G. Burkard, *Phys. Rev. B* **74**, 174510 (2006).
- [16] R. P. Tiwari and D. Stroud, *Phys. Rev. B* **76**, 220505 (2007).
- [17] R. Leone, L. P. Lévy, and P. Lafarge, *Phys. Rev. Lett.* **100**, 117001 (2008).
- [18] R.-P. Riwar, M. Houzet, J. S. Meyer, and Y. V. Nazarov, *Nature Communications* **7**, 11167 (2016).
- [19] E. V. Repin and Y. V. Nazarov, arXiv e-prints, arXiv:2010.11494 (2020), arXiv:2010.11494 [cond-mat.mes-hall].
- [20] Y. Makhlin, G. Schön, and A. Shnirman, *Rev. Mod. Phys.* **73**, 357 (2001).
- [21] R. F. G. Falci, E. Paladino, “Quantum phenomena of mesoscopic systems,” (IOS Press, 2003).
- [22] L. Chiroli and G. Burkard, *Advances in Physics* **57**, 225 (2008), <https://doi.org/10.1080/00018730802218067>.
- [23] J. Koch, T. M. Yu, J. Gambetta, A. A. Houck, D. I. Schuster, J. Majer, A. Blais, M. H. Devoret, S. M. Girvin, and R. J. Schoelkopf, *Phys. Rev. A* **76**, 042319 (2007).
- [24] J. A. Schreier, A. A. Houck, J. Koch, D. I. Schuster, B. R. Johnson, J. M. Chow, J. M. Gambetta, J. Majer, L. Frunzio, M. H. Devoret, S. M. Girvin, and R. J. Schoelkopf, *Phys. Rev. B* **77**, 180502 (2008).
- [25] R. Barends, J. Kelly, A. Megrant, D. Sank, E. Jeffrey, Y. Chen, Y. Yin, B. Chiaro, J. Mutus, C. Neill, P. O’Malley, P. Roushan, J. Wenner, T. C. White, A. N. Cleland, and J. M. Martinis, *Phys. Rev. Lett.* **111**, 080502 (2013).
- [26] R. Bistritzer and A. H. MacDonald, *Proceedings of the National Academy of Sciences* **108**, 12233 (2011), <https://www.pnas.org/content/108/30/12233.full.pdf>.
- [27] Y. Cao, V. Fatemi, A. Demir, S. Fang, S. L. Tomarken, J. Y. Luo, J. D. Sanchez-Yamagishi, K. Watanabe, T. Taniguchi, E. Kaxiras, R. C. Ashoori, and P. Jarillo-Herrero, *Nature* **556**, 80 (2018).
- [28] Y. Cao, V. Fatemi, S. Fang, K. Watanabe, T. Taniguchi, E. Kaxiras, and P. Jarillo-Herrero, *Nature* **556**, 43 (2018).
- [29] A. Kitaev, arXiv e-prints, cond-mat/0609441 (2006), arXiv:cond-mat/0609441 [cond-mat.mes-hall].
- [30] A. Gyenis, P. S. Mundada, A. Di Paolo, T. M. Hazard, X. You, D. I. Schuster, J. Koch, A. Blais, and A. A. Houck, arXiv e-prints, arXiv:1910.07542 (2019), arXiv:1910.07542 [quant-ph].
- [31] T. W. Larsen, K. D. Petersson, F. Kuemmeth, T. S. Jespersen, P. Krogstrup, J. Nygård, and C. M. Marcus, *Phys. Rev. Lett.* **115**, 127001 (2015).

- [32] F. Luthi, T. Stavenga, O. W. Enzing, A. Bruno, C. Dickel, N. K. Langford, M. A. Rol, T. S. Jespersen, J. Nygård, P. Krogstrup, and L. DiCarlo, *Phys. Rev. Lett.* **120**, 100502 (2018).
- [33] P. Krogstrup, N. L. B. Ziino, W. Chang, S. M. Albrecht, M. H. Madsen, E. Johnson, J. Nygård, C. M. Marcus, and T. S. Jespersen, *Nature Materials* **14**, 400 (2015).
- [34] D. J. van Woerkom, A. Proutski, B. van Heck, D. Bouman, J. I. Väyrynen, L. I. Glazman, P. Krogstrup, J. Nygård, L. P. Kouwenhoven, and A. Geresdi, *Nature Physics* **13**, 876 (2017).
- [35] G. Blatter, V. B. Geshkenbein, and L. B. Ioffe, *Phys. Rev. B* **63**, 174511 (2001).
- [36] B. Douçot and J. Vidal, *Phys. Rev. Lett.* **88**, 227005 (2002).
- [37] I. V. Protopopov and M. V. Feigel'man, *Phys. Rev. B* **70**, 184519 (2004).
- [38] S. Gladchenko, D. Olaya, E. Dupont-Ferrier, B. Douçot, L. B. Ioffe, and M. E. Gershenson, *Nature Physics* **5**, 48 (2009).
- [39] M. T. Bell, J. Paramanandam, L. B. Ioffe, and M. E. Gershenson, *Phys. Rev. Lett.* **112**, 167001 (2014).
- [40] K. Kalashnikov, W. T. Hsieh, W. Zhang, W.-S. Lu, P. Kamenov, A. Di Paolo, A. Blais, M. E. Gershenson, and M. Bell, *PRX Quantum* **1**, 010307 (2020).
- [41] Y. Nakamura, Y. A. Pashkin, T. Yamamoto, and J. S. Tsai, *Phys. Rev. Lett.* **88**, 047901 (2002).
- [42] S. M. Anton, C. Müller, J. S. Birenbaum, S. R. O'Kelley, A. D. Fefferman, D. S. Golubev, G. C. Hilton, H.-M. Cho, K. D. Irwin, F. C. Wellstood, G. Schön, A. Shnirman, and J. Clarke, *Phys. Rev. B* **85**, 224505 (2012).
- [43] N. Didier, E. A. Sete, M. P. da Silva, and C. Rigetti, *Phys. Rev. A* **97**, 022330 (2018).
- [44] S. A. Caldwell, N. Didier, C. A. Ryan, E. A. Sete, A. Hudson, P. Karalekas, R. Manenti, M. P. da Silva, R. Sinclair, E. Acala, N. Alidoust, J. Angeles, A. Bestwick, M. Block, B. Bloom, A. Bradley, C. Bui, L. Capelluto, R. Chilcott, J. Cordova, G. Crossman, M. Curtis, S. Deshpande, T. E. Bouayadi, D. Girshovich, S. Hong, K. Kuang, M. Lenihan, T. Manning, A. Marchenkov, J. Marshall, R. Maydra, Y. Mohan, W. O'Brien, C. Osborn, J. Otterbach, A. Papageorge, J.-P. Paquette, M. Pelstring, A. Polloreno, G. Prawiroatmodjo, V. Rawat, M. Reagor, R. Renzas, N. Rubin, D. Russell, M. Rust, D. Scarbelli, M. Scheer, M. Selvanayagam, R. Smith, A. Staley, M. Suska, N. Tezak, D. C. Thompson, T.-W. To, M. Vahidpour, N. Vodrahalli, T. Whyland, K. Yadav, W. Zeng, and C. Rigetti, *Phys. Rev. Applied* **10**, 034050 (2018).